Anbar Journal of Engineering Science (AJES)
P-ISSN: 1997-9428; E-ISSN: 2706-7440

Vol. 12 , No. 1 (2021) , pp. 65 ~ 75
DOI: 10.37649/aengs.2021.171199

Unviersty of Anbar

Anbar Journal Of Engineering Science©

journal homepage: http://www.uoanbar.edu.iq/Evaluate/

Numerical Investigation on heat transfer enhancement and entropy generation in a triangular ribbed-channel using nanofluid

Mohammad N. Dahham [a]*, M. A. Ahmed [a]

[a] Department of Mechanical Engineering, College of Engineering, University of Anbar Ramadi, Anbar, Iraq

P A P E R I N F O

Paper history:
Received 15/2/2021
Revised 29/3/ 2021
Accepted 13/4/ 2021

Keywords:
Triangular ribs
Thermal-hydraulic performance
Turbulent Flow
Nanofluids
Entropy generation

A B S T R A C T

In this paper, turbulent convective heat transfer in a triangular-ribbed channel has been numerically investigated. SiO_2-water with nanoparticles volume fraction of 4% and nanoparticles diameters of 30 nm is employed with Reynolds number ranging from 2000 to 8000. The governing continuity, momentum and energy equations in addition to low Reynolds number k-ε model have been transformed into body-fitted coordinates system and then solved using finite volume method. The effects of Reynolds number and rib heights on Nusselt number, pressure drop, thermal-hydraulic performance factor and entropy generation are presented and discussed. It is observed that the Nusselt number, pressure drop and thermal performance increase with increasing of Reynolds number and rib height. In addition, the highest performance factor can be obtained at Reynolds number of 6500 and rib height of 1.5 mm.

1. Introduction

In most practical applications, research on techniques for heat transfer augmentation has become very essential to design heat exchangers with high performance and more compact in size. Therefore, using nanofluid as working fluids in a ribbed-channel may lead to significant improvement in the thermal performance of such heat exchangers. Many researchers have been previously investigated the problem of turbulent forced convection flow in channels with different shapes. Habib et al. [1] performed a numerical study on the characteristics of turbulent convective heat transfer in a rectangular duct with staggered baffles. Results showed that the local and average heat transfer coefficient as well as the pressure losses increase with the baffle height and Reynolds number. Turbulent flows and heat transfer behavior in a three dimensional rectangular-ribbed channel with longitudinal vortex generators has been numerically investigated by Zhu et al. [2].Numerical results showed that the combined effect of the rib- roughness as well as the vortex generators can improve the rate of heat transfer about 450% as a compared with the smooth channel. Yang and Hwang [3] numerically investigated on the convective heat transfer in channel with porous baffles over Reynolds number range of 10000 - 50000. The finite difference method was used to solve the turbulent governing equations based on SIMPLE algorithm. It is found that the averaged Nusselt number increases as the baffle height in-

* Corresponding author. **Mohammad N. Dahham** : mohammad.dahham@gmail.com ; +9647823155678

creases. Naphon [4] experimentally investigated on the convective heat transfer characteristics in a V-corrugated channel over Reynolds number range of 2000 - 9000. It was observed that the corrugated surface has a clear effect on the average Nusselt number as well as the pressure drop penalty in comparison with smooth channel. Promvonge and Thianpong [5] experimentally investigated on the behavior of turbulent convective heat transfer in a ribbed channel using air as a working fluid. Experiments were conducted for Reynolds number range of 4000 - 16000. Results showed that the in-line rib arrangement displays higher heat transfer rate and pressure losses than the staggered arrangement at a given Reynolds number. Elshafei et al. [6] experimentally investigated on the turbulent forced convection flow in a triangular-corrugated channel over Reynolds number range of 3220- 9420. It was found that the corrugated channels can provide a significant heat transfer augmentation with increasing in the pressure drop penalty compared with smooth channels. Zhang and Che [7] numerically investigated of turbulent forced convection flow in corrugated channel with different shapes using finite volume method. It is found that the trapezoidal channel displays the highest thermal-hydraulic performance as a compared with the other shapes of channel. Manca et al. [8] numerically studied on the heat transfer enhancement in a ribbed channel using Al_2O_3 – water nanofluid. The simulation were carried out for Reynolds numbers ranging from 20000 to 60000. Results showed that the rate of heat transfer enhancement increases with the concentration of nanoparticles but it accompanied with increasing the pressure drop penalty. Ahmed et al. [10-15] numerically and experimentally studied on the heat transfer enhancement in corrugated (wavy) channels with different shapes using nanofluids. Results showed that average Nusselt number increases with increasing the amplitude of corrugated (wavy) channel as well as with the nanoparticles volume fraction. It is also observed that the corrugated (wavy) channels with various shapes display the highest heat transfer rate in comparison with the smooth channel. Vanaki and Mohammed [16] numerically investigated on the turbulent forced convection of nanofluid flow in channel with different rib shapes over Reynolds number range of 5000-20000. Results showed that the triangular-ribbed channel can displayed the best performance as a compared with the other shapes of ribs. Ahmed [17] numerically studied of hydrothermal behavior of nanofluid flow in a channel with triangular baffles using finite volume method. The computations were carried out for Reynolds number range of 5000-10000. Results showed that the rate of heat transfer and the friction losses increase with the height of baffles. Rashidi et al. [18] numerically investigated on heat transfer enhancement and entropy generation analysis in a corrugated channel over Reynolds number range of 5000-50000. Results showed that the minimum value of entropy generation has been obtained at Re = 20000 for a given values of wavelength and amplitude of the corrugated channel. The corrugated channel with a wave amplitude of 0.1 provide the highest thermal performance at a given Reynolds number. Wang et al. [19] numerically studied on entropy generation analysis of turbulent convective heat transfer in helically corrugated tubes. The computations were conducted for Reynolds number range of 10020-40060. It is observed that both the average heat transfer and friction entropy generations increase with increasing Reynolds number as well as corrugation height and decreasing corrugation pitch. Fadodun et al. [20] numerically investigated on the entropy generation behavior for the convective turbulent flow in a corrugated pipe using nanofluid. The simulation were carried out for Reynolds number range of 5000- 40000 and nanoparticle concentration range of 0- 0.25%. Results showed that with increasing the amplitude of corrugation as well as nanoparticles concentration, the viscous entropy generation increases while thermal entropy generation decreases

In current paper, a numerical investigation based on the finite volume approach has been conducted to study the turbulent convective heat transfer SiO_2-water nanofluid in a triangular-ribbed channel. Effects of the rib height and Reynolds number on the flow and thermal behavior are presented and analyzed.

2. Mathematical formulation

2.1 Problem description and asumptions

A schematic diagram of the geometric model considered in the current study is shown in Fig. 1. A triangular- ribbed channel has been considered with channel height (H) of 10 mm, and length (L) of 460 mm. The channels consist of three sections including a heated section (ribbed walls) with length (L_2) of 110 mm which is heated with a constant heat flux (300 W/m^2), adiabatic developing section with length (L_1) of 250 mm and adiabatic exit section with length (L_3) of 100 mm. The ribs have uniform dimensions with heights (a) of 0.5, 1 and 1.5 mm and rib-to-rib space of (p) of 5 mm and width of (b) 2 mm. A fifteen ribs have been used at each wall of channel .A uniform heat flux conditions is applied to the heated walls with no slip conditions. It can be

assumed that the flow is two-dimensional, steady, turbulent and incompressible. Furthermore, SiO_2 - water nanofluid is assumed as a homogenous mixture.

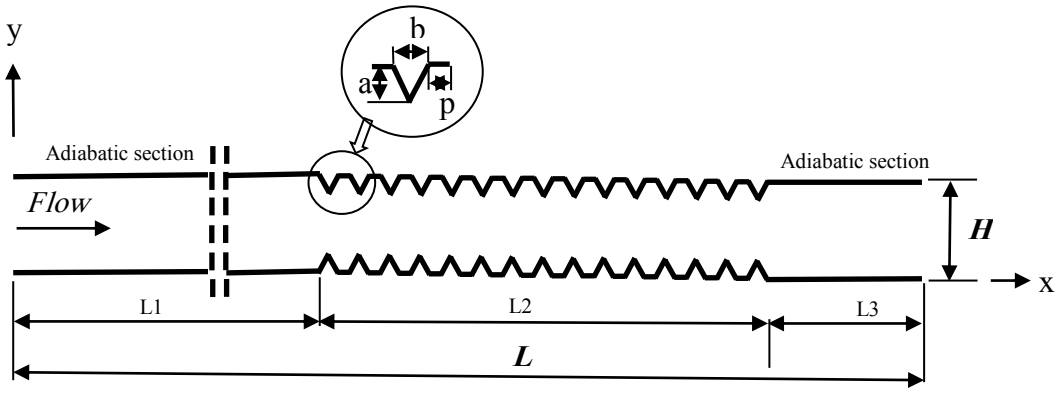

Fig. 1. Geometric model of current study.

2.2. Governing equations and boundary conditions

The two-dimensional governing continuity momentum and energy equations can be expressed as [17]:

Continuity equation:

$$\frac{\partial}{\partial x}(\rho u)+\frac{\partial}{\partial y}(\rho v)=0 \quad (1)$$

X-Momentum equation:

$$\frac{\partial}{\partial x}(\rho uu)+\frac{\partial}{\partial y}(\rho vu)=-\frac{\partial p}{\partial x}+\frac{\partial}{\partial x}\left[(\mu+\mu_t)\frac{\partial u}{\partial x}\right]+\frac{\partial}{\partial y}\left[(\mu+\mu_t)\frac{\partial u}{\partial y}\right]+\frac{\partial}{\partial x}\left[(\mu+\mu_t)\frac{\partial u}{\partial x}-\frac{2}{3}\rho k\right]+\frac{\partial}{\partial y}\left[(\mu+\mu_t)\frac{\partial v}{\partial x}\right] \quad (2)$$

Y-momentum equation:

$$\frac{\partial}{\partial x}(\rho uv)+\frac{\partial}{\partial y}(\rho vv)=-\frac{\partial p}{\partial y}+\frac{\partial}{\partial x}\left[\left(\mu+\mu_t\right)\frac{\partial v}{\partial x}\right]+\frac{\partial}{\partial y}\left[\left(\mu+\mu_t\right)\frac{\partial v}{\partial y}\right]+\frac{\partial}{\partial x}\left[\left(\mu+\mu_t\right)\frac{\partial u}{\partial y}\right]+\frac{\partial}{\partial y}\left[\left(\mu+\mu_t\right)\frac{\partial v}{\partial y}-\frac{2}{3}\rho k\right] \quad (3)$$

Energy equation:

$$\frac{\partial}{\partial x}(\rho uT)+\frac{\partial}{\partial y}(\rho vT)=\frac{\partial}{\partial x}\left[\left(\frac{K}{C_p}+\frac{\mu_t}{\mathrm{Pr}_t}\right)\frac{\partial T}{\partial x}\right]+\frac{\partial}{\partial y}\left[\left(\frac{K}{C_p}+\frac{\mu_t}{\mathrm{Pr}_t}\right)\frac{\partial T}{\partial y}\right] \quad (4)$$

Turbulence model used to estimate the turbulent viscosity can be defined as [21]:

Turbulent kinetic energy (k) equation:

$$\frac{\partial}{\partial x}(\rho uk)+\frac{\partial}{\partial y}(\rho vk)=\frac{\partial}{\partial x}\left[\Gamma_k\frac{\partial k}{\partial x}\right]+\frac{\partial}{\partial y}\left[\Gamma_k\frac{\partial k}{\partial y}\right]+P_k-\rho(\varepsilon+\varepsilon_w) \quad (5)$$

Where ε_w is the dissipation rate at the wall and it can be defined as:

$$\varepsilon_w=2\frac{\mu}{\rho}\left[\left(\frac{\partial\sqrt{k}}{\partial x}\right)^2+\left(\frac{\partial\sqrt{k}}{\partial y}\right)^2\right] \quad (6)$$

Turbulent kinetic energy dissipation (ε) equation:

$$\frac{\partial}{\partial x}(\rho u\varepsilon)+\frac{\partial}{\partial y}(\rho v\varepsilon)=\frac{\partial}{\partial x}\left[\Gamma_\varepsilon\frac{\partial\varepsilon}{\partial x}\right]+\frac{\partial}{\partial y}\left[\Gamma_\varepsilon\frac{\partial\varepsilon}{\partial y}\right]+(C_1 f_1 P_k-\rho C_2 f_2\varepsilon)\frac{\varepsilon}{k}+\phi_\varepsilon \quad (7)$$

Where

$$\phi_\varepsilon = 2\mu_t \frac{\mu}{\rho}\left[\left(\frac{\partial^2 u}{\partial x^2}\right)^2 + \left(\frac{\partial^2 v}{\partial x^2}\right)^2 + 2\left(\frac{\partial^2 u}{\partial x \partial y}\right)^2 + 2\left(\frac{\partial^2 v}{\partial x \partial y}\right)^2 + \left(\frac{\partial^2 u}{\partial y^2}\right)^2 + \left(\frac{\partial^2 v}{\partial y^2}\right)^2\right] \quad (8)$$

The production rate of the turbulent kinetic energy (p_k) in Eq. (7) can be expressed as:

$$p_k = \mu_t \left\{2\left[\left(\frac{\partial u}{\partial x}\right)^2 + \left(\frac{\partial v}{\partial y}\right)^2\right] + \left(\frac{\partial u}{\partial y} + \frac{\partial v}{\partial x}\right)^2\right\} - \frac{2}{3}\rho k\left(\frac{\partial u}{\partial x} + \frac{\partial v}{\partial y}\right) \quad (9)$$

Therefore, the turbulent viscosity can be estimated as [21]:

$$\mu_t = C_\mu f_\mu \rho \frac{k^2}{\varepsilon} \quad (10)$$

The empirical constants and the turbulent Prandtl number are given as [21]:

$$C_\mu = 0.09,\ C_1 = 1.44,\ C_2 = 1.92,\ \sigma_k = 1.0,\ \sigma_\varepsilon = 1.3,\ \mathrm{Pr}_t = 0.9 \quad (11)$$

The wall-damping functions and the turbulent Reynolds number are [22]:

$$f_1 = 1.0 \quad (12)$$

$$f_2 = 1 - 0.3\exp\left(-\mathrm{Re}_T^2\right) \quad (13)$$

$$f_\mu = exp\left[-3.4/\left(1 + 0.02\,Re_T\right)^2\right] \quad (14)$$

$$\mathrm{Re}_T = \frac{\rho}{\varepsilon}\frac{k^2}{\mu} \quad (15)$$

The corresponding boundary conditions used to solve the current problems can be expressed as [17]:

-Inlet flow:

$$u = u_{in}, v = 0, \qquad T = T_{in}, \qquad k = k_{in} = \frac{2}{3}\left(I_o\, u_{in}\right)^2,$$

$$\varepsilon = C\mu^{3/4}\, k_{in}^{3/2} /(0.07 D_h) \quad (16)$$

-Outlet flow:

$$\frac{\partial \mathrm{u}}{\partial \mathrm{x}} = 0,\ \frac{\partial \mathrm{v}}{\partial \mathrm{x}} = 0,\ \frac{\partial \mathrm{T}}{\partial \mathrm{x}} = 0,\ \frac{\partial \mathrm{k}}{\partial \mathrm{x}} = 0,\ \frac{\partial \varepsilon}{\partial \mathrm{x}} = 0 \quad (17)$$

-Along the channel walls:

$$u = 0,\ v = 0,\ k = 0,\ \varepsilon = 0 \quad (18)$$

$$\left.\frac{\partial T}{\partial y}\right|_w = -\frac{q_w}{K} \quad (19)$$

along heated-ribbed walls

$$\left.\frac{\partial \mathrm{T}}{\partial \mathrm{y}}\right|_{\mathrm{w}} = 0 \quad (20)$$

along adiabatic- smooth walls

-Local and average entropy generation equations can be expressed as [23]:

$$S_g = \frac{K}{T^2}\left[\left(\frac{\partial T}{\partial x}\right)^2 + \left(\frac{\partial T}{\partial y}\right)^2\right] + \frac{\mu_{eff}}{T}\left\{2\left[\left(\frac{\partial u}{\partial x}\right)^2 + \left(\frac{\partial v}{\partial x}\right)^2\right] + \left[\left(\frac{\partial u}{\partial y}\right) + \left(\frac{\partial v}{\partial x}\right)\right]^2\right\} \quad (21)$$

$$N_t = \int N_g\, dx \quad (22)$$

Where $N_g$is the dimensionless rate of entropy generation, which can be given as [23]:

$$N_g = \frac{S_g\ D_h^2}{K} \quad (23)$$

The local and average Nusselt numbers can be defined as follows [17]:

$$Nu_x = \frac{D_h}{K}\frac{q_w}{(T_w - T_b)} \quad (24)$$

$$Nu_{av} = \frac{1}{L_2}\int_{L_1}^{L_1+L_2} Nu_x\, dx \quad (25)$$

Where T_b is the bulk fluid temperature, which can be determined as follows [17]:

$$T_b = \frac{\iint_A \rho u C_p T\, dA}{\iint_A \rho u C_p\, dA} \quad (26)$$

The thermal-hydraulic performance factor is defined as [17]:

$$\mathrm{PEC} = \frac{(Nu_{av}/\,Nu_{av,s})}{(f/\,f_s)^{1/3}} \tag{27}$$

Where f is the friction factor, which can be expressed as [17]:

$$f = \Delta P \,\frac{D_h}{L}\frac{2}{\rho_{nf}\,u_{in}^2} \tag{28}$$

The thermophysical properties of SiO_2-water nanofluid considered in the present study are the ones used by Navaei et al. [24].

3. Numerical algorithm

A CFD program based on FORTRAN 90 has been developed to simulate the current problem. The governing equations are solved using the finite volume method based on the SIMPLE algorithm [25]. The convection terms, in the governing equations, are discretized using upwind scheme, while the diffusion terms are discretized using second-order central differencing scheme. The two Poisson equations are adopted to develop the computational mesh. The physical variables are stored at the same nodes of the computational mesh using collocated grid arrangement [26]. The under-relaxation is adopted for all physical variables in order to achieve the solution convergence. Therefore, the convergence criterion for each variable is set to 10^{-4}.

4. Code validation and grid independence test

In order to check the accuracy and the validation of the CFD code developed in the present study, the average Nusselt number and friction factor for AL_2O_3-water nanofluid flow in a triangular-ribbed channel have been investigated and compared with the numerical results for Vanaki and Mohammed [16]. It was found that the maximum deviations for the Nusselt number and the friction factor are 3.5 % and 4.8 %, respectively, as shown in Fig. 2. For the grid independence test, the average Nusselt number has been investigated for the SiO_2-water nanofluid in the channel with triangular ribs (a=1.5 mm, p=5 mm, φ = 4% ,and dp=30 nm), see Fig. 3. It is observed that grid size of (601x101) can provide the grid-independent solution.

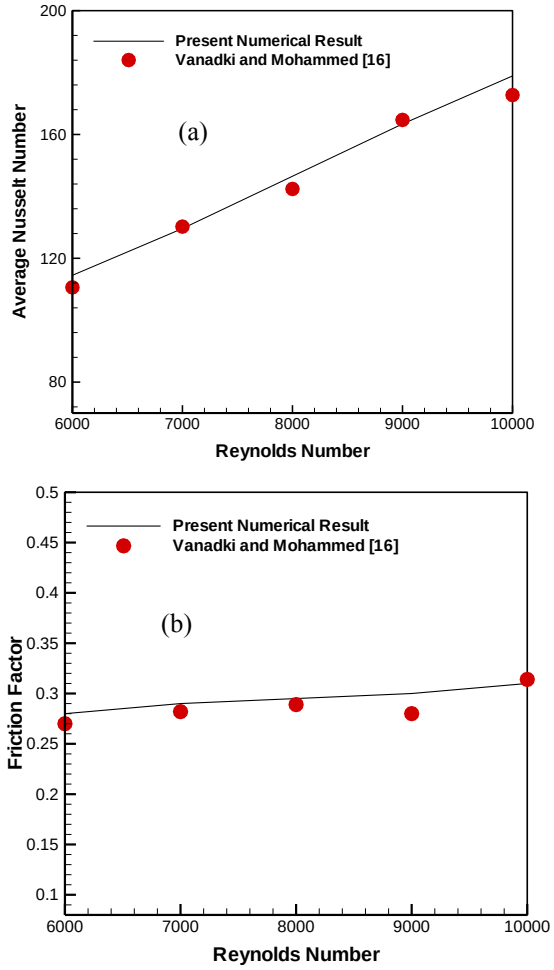

Fig. 2. Comparison of the numerical results of current study with a previous numerical study for Vanaki and Mohammed [16] : (a) average Nusselt number, (b) friction factor.

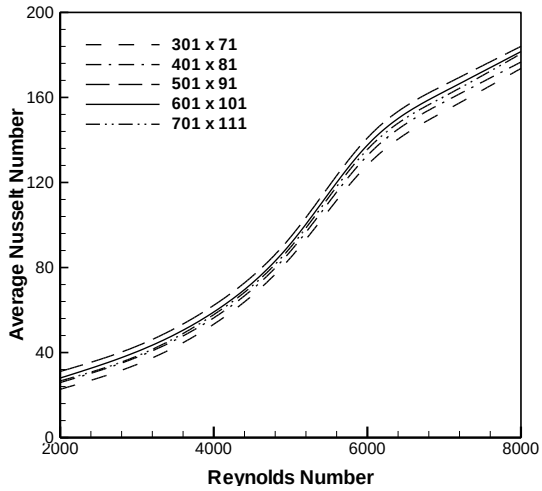

Fig. 3. Average Nusselt number vs. Reynolds number for different grid sizes.

5. Results and discussion

The effect of Reynolds number on the streamwise velocity, isotherms and total entropy generation contours for triangular-ribbed channels using SiO_2-water nanofluid at φ = 4%, dp=30 nm, a = 1.5 mm, p = 5 mm are shown in Fig. 5. In general, it can be seen that all the contours are symmetric about (x-direction). When the fluid flow in a ribbed channel, the recirculation regains began growing laterally along the walls of channel. The direction of velocity in these regions in the opposite direction to the main flow. As Reynolds number increases, the intensity and sizes of these regions increase, see Fig. 5 a. From isotherms contours, it can be seen that the temperature gradient at the ribbed-walls increases with Reynolds number. This because improve the mixing of the cold fluid in core with the hot fluid near the walls due to grow the re-circulation regions near the walls. Therefore, the thickness of thermal boundary layers decreases because of increasing the Reynolds number. It also found that the maximum value of entropy generation occurs at the walls of channel due to the effects of velocity and temperature gradients. The value of entropy generation for the core fluid is lower than that at the walls due to low temperature gradient.

Fig. 6 (a) displays the streamwise velocity contours for triangular-ribbed channel with different values of the rib height. It can be observed that the size of re-circulation regions increase with the rib height, hence, this led to increase the intensity of these regions to the main flow. The effect of rib height on the isotherm contours are shown in Fig. 6 (b). As rib height increase, the thickness of the thermal boundary layers increase. This because of the size re-circulation region that appear near the walls increase with height and increase the temperature gradient as well as the heat transfer rate. Fig. 6 (c) depicts the effect of rib height on the total entropy generation contours. It can be seen that the total entropy generation about zero at the central core of channel for all values of rib due to velocity and temperature gradient at center line of channel. While, the highest value of the total entropy generation observed at walls of the channel due to increase the velocity as well as the temperature gradient. As the rib height increases, the value of entropy generation increases. This is due to the effect of the recirculation region that grow near the walls of the channel.

Fig. 7 shows the variation of the average Nusselt number with Reynolds numbers for different rib height at p= 5 mm. It can be seen that the rib height have significant effects on the average Nusselt numbers especially at high Reynolds number. It is found that the average Nusselt number increasing with the increases of the ribs height as well as Reynolds number. This is due to the effect of the recirculation region that appears in the channel and hence this led to improve the heat transfer rate. The smooth channel (i.e. a=0) displays a lowest value of Nusselt number due to pure fluid mixing in such channel. Fig. 8 displays the effect of rib height on the pressure drop for different Reynolds number at p= 5 mm. It can be seen that the pressure drop increase with Reynolds number, as expected, due to the increase the velocity gradient with the Reynolds number. Furthermore, the pressure drop increase with the rib height due to the increase the intensity of recirculation region that grows in channel. The smooth channel displays the smallest value of the pressure drop. This is because the flow in the smooth channel regular and there is no circulation.

Fig. 9 shows the effect of the ribs height on the total entropy generation with different Reynolds numbers. In general, the entropy generation decreased with increasing of Reynolds number. It also found that the total entropy generation increase with rib height due to the effect of recirculation regions that appear in a ribbed channel near the walls and hence increase total entropy generation. Fig. 10 illustrates the variation of performance factor with rib height at p= 5 mm. It can be seen that the performance factor is a greater than unity for all values of ribs height. This means that the argumentation in heat transfer is great than the increasing in pressure drop.

6. Conclusion

In this paper, turbulent convective heat transfer in a triangular-ribbed channel has been numerically investigated over Reynolds number range of 2000-8000. SiO_2-water with nanoparticles volume fraction of 4% and nanoparticles diameters of 30 nm has been considered. The governing continuity, momentum and energy equations in addition to low Reynolds number k-ε model have been solved using finite volume approach. The effects of Reynolds number and rib heights on Nusselt number, pressure drop, thermal-hydraulic performance factor and entropy generation are investigated and discussed. It is observed that the Nusselt number, pressure drop, total entropy generation and thermal

performance increase with increasing rib height. It is found that maximum value of thermal-hydraulic performance is 3.8 at Re=6500, a=1.5mm and p=5mm.Generally, the result of the current study shows that the using nanofluid and ribbed channel can be enhanced that the thermal-hydraulic performance with more compact design of heat exchangers.

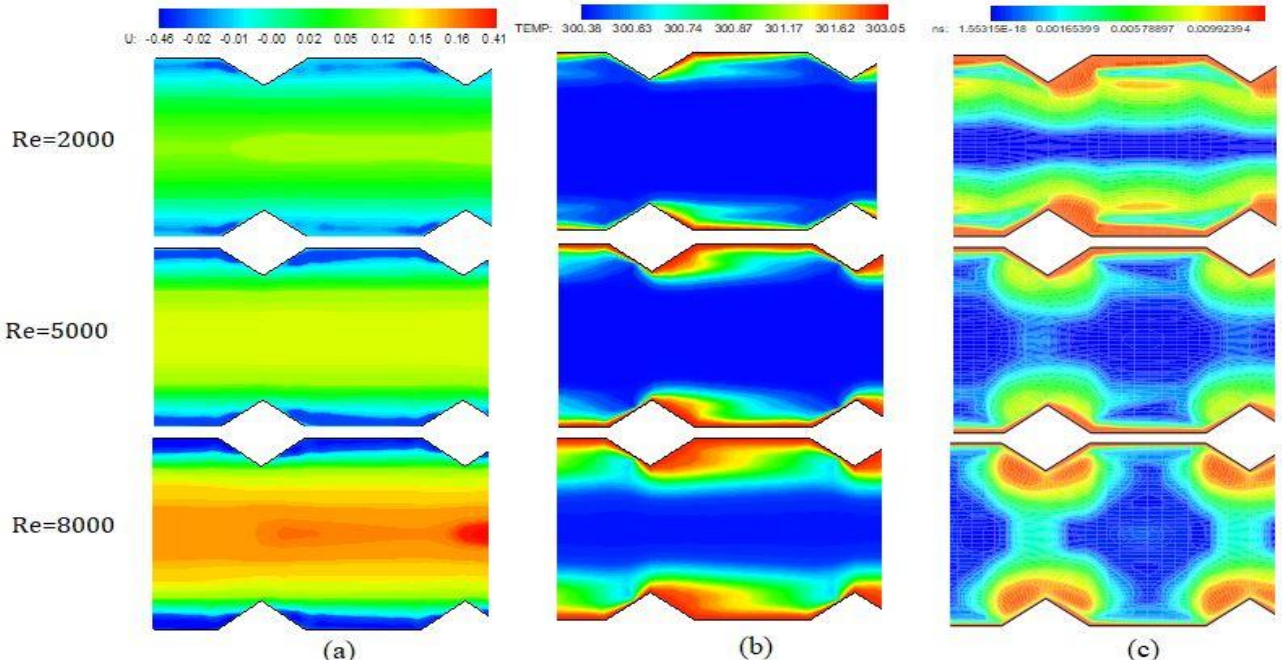

Fig.5**.** (a) Streamwise velocity contours, (b) isotherms contours and (c) total entropy generation contours for different Reynolds number at a=1.5 mm and p=5 mm.

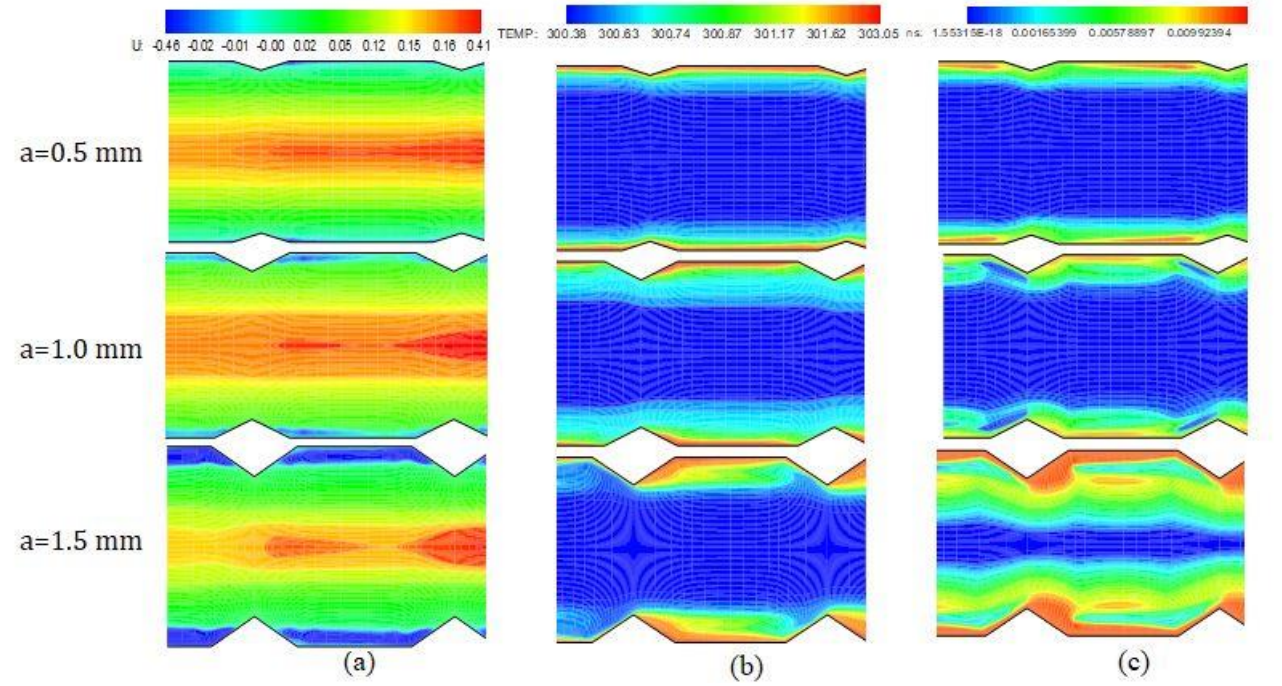

Fig.6. Streamwise velocity contours, (b) isotherms contours and (c) total entropy generation contours for different rib height at Re= 8000 and p=5 mm.

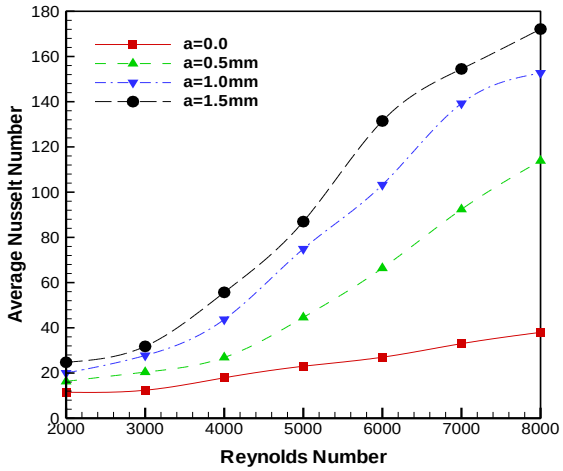

Fig. 7. Average Nusselt number vs. Reynolds number for different rib heights at p= 5 mm.

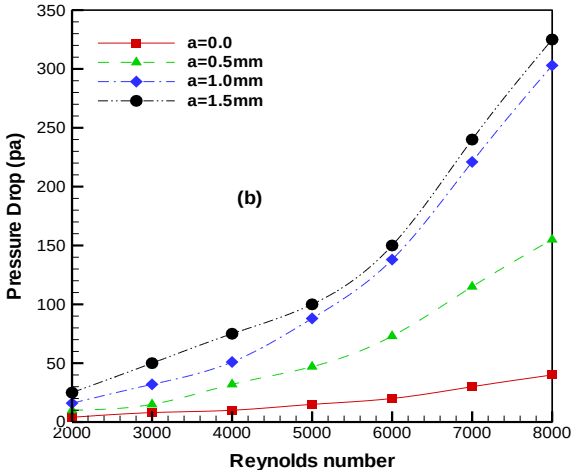

Fig. 8. Pressure drop vs. Reynolds number for different rib heights at p= 5 mm.

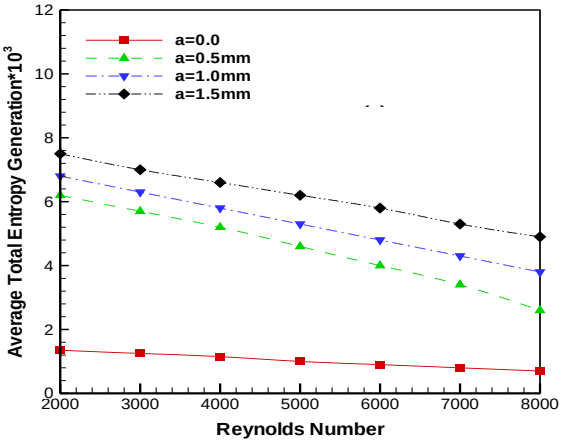

Fig. 9. Average total entropy generation vs. Reynolds number for different rib heights at p= 5 mm.

[5] P. Promvonge and C. Thianpong, Thermal performance assessment of turbulent channel flows over Different shaped ribs, Int. commun. in heat and mass transfer 35 (2008) 1327-1334.
[6] E.A.M. Elshafei, M.M. Awad, E.El-Negiry and A.G.Ali , Heat transfer and pressure drop in corrugated channels, Energy 35 (2010) 101-110.
[7] L. Zhang and D. Che, Influence of corrugation profile on the thermal hydraulic performance of cross-corrugated plates, Numerical Heat Transfer, Part A: Applications, 59(2011) 267-296.
[8] O. Manca, S. Nardini, and D. Ricci, A numerical study of nanofluid forced convection in ribbed channels, Applied Thermal Engineering, 37 (2012) 280-292.

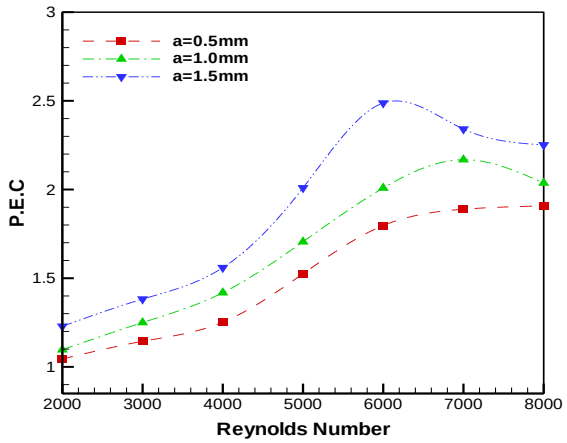

Fig. 10**.** Performance factor vs. Reynolds number for different rib heights at p= 5 mm.

References

[1] M.A. Habib, A.M. Mobarak, M.A. Sallak, E.A. Abdel Hadi, R.I. Affify, Experimental investigation of heat transfer and flow over baffles of different heights, ASME J. Heat Transf. 116 (1994) 363–368.
[2] J. X. Zhu, M. Fiebig and N. K. Mitra, Numerical investigation of turbulent flows and heat transfer in a rib-roughened channel with longitudinal vortex generators. Int. J. Heat and Mass Transfer 38 (1995) 495-501.
[3] Y.T. Yang, C.Z. Hwang, Calculation of turbulent flow and heat transfer in a porous baffled channel, Int. J. Heat Mass Transfer 46 (2003) 771–780.
[4] P. Naphon, Heat transfer characteristics and pressure drop in channel with V corrugated upper and lower plates, Energy conversion and management 48 (2007) 1516-1524.
[9] M. A. Ahmed, N. H. Shuaib, M. Z. Yusoff and A. H. Al-Falahi, Numerical investigations of flow and heat transfer enhancement in a corrugated channel using nanofluid, Int. Commun. Heat Mass Transfer, 38 (2011) 1368-1375.
[10] M. A. Ahmed, N. H. Shuaib and M. Z. Yusoff, Numerical investigations on the heat transfer enhancement in a wavy channel using nanofluid, *Int. J.Heat and Mass Transfe,* 55 (2012) 5891-5898.
[11] M. A. Ahmed, M. Z. Yusoff, and N. H. Shuaib, Effects of geometrical parameters on the flow and heat transfer characteristics in trapezoidal-corrugated channel using nano fluid, Int. Commun. Heat Mass Transf., 42 (2013) 69-74.
[12] M. A. Ahmed, M. Z. Yusoff, K. C. Ng, and N. H.Shuaib, Effect of corrugation profile on the thermal–hydraulic performance of cor-

rugated channels using CuO–water nanofluid, *Case Studies in Thermal Engineering* 4 (2014) 65-75.

[13] M. A. Ahmed, M. Z. Yusoff, K. C. Ng, and N. H.Shuaib, Numerical and experimental investigations on the heat transfer enhancement in corrugated channels using SiO_2–water nanofluid" Case Studies in Thermal Engineering, 6 (2015) 77-92.

[14] M. A. Ahmed, M. Z. Yusoff, K. C. Ng, and N. H.Shuaib, The effects of wavy-wall phase shift on thermal-hydraulic performance of Al_2O_3–water nanofluid flow in sinusoidal-wavy channel, *Case Studies in Thermal Engineering* 4 (2014) 153-165.

[15] M. A. Ahmed, M. Z. Yusoff, K. C. Ng, and N. H.Shuaib, Numerical investigations on the turbulent forced convection of nanofluids flow in a triangular-corrugated channel, *Case Studies in Thermal Engineering* 6 (2015) 212-225.

[16] M. A. Ahmed, Numerical Study of Turbulent Thermal-Hydraulic Performance of Al_2O_3-Water Nanofluid in Channel with Triangular Baffles, Anbar Journal of Engineering Science, 7 (2016) 9-20.

[17] S. Rashidi, M. Akbarzadeh, R. Masoodi and E. M. Languri, Thermal-hydraulic and entropy generation analysis for turbulent flow inside a corrugated channel, Int. J. Heat and Mass Transfer 109 (2017) 812-823.

[18] W. Wang, Y. Zhang, J. Liu, Z. Wu, B. Li and B. Sundén, Entropy generation analysis of fully developed turbulent heat transfer flow in inward helically corrugated tubes. Numerical Heat Transfer, Part A: Applications, 73(2018) 788-805.

[19] O. G. Fadodun, A. A. Amosun, N. L. Okoli, D. O. Olaloye, J. A. Ogundeji and S.S. Durodola, Numerical investigation of entropy production in SWCNT/H2O nanofluid flowing through inwardly corrugated tube in turbulent flow regime, J. Thermal Analysis and Calorimetry, 11 (2020) 1-16.

[20] J. Blazek, Computational Fluid Dynamics: Principles and Applications: Principles and Applications, 2nd edition. Elsevier, 2005.

[21] C. J. Chen, S.Y. Jaw, Fundamentals of turbulence modelling, Taylor and Francis, 1997.

[22] D. Bijan, S. Rashidi and J. A.Esfahani, Sensitivity analysis of entropy generation in nanofluid flow inside a channel by response surface methodology, Entropy 18 (2016) 1-16.

[23] A.S. Navaei, H.A. Mohammed, K.M. Munisamy, H. Yarmand, S. Gharehkhani, Heat transfer enhancement of turbulent nanofluid flow over various types of internally corrugated channels, Powder Technology 286 (2015) 332–341.

[24] H.K Versteeg & Malalasekera, *"An Introduction to Computational Fluid Dynamics the finite volume method,"* 2nd ed., vol. M. England: Longman Scientific and Technica, 2007.

[25] J. H. Ferziger and M. Peric, *Computational methods for fluid dynamics*, vol. 46, no. 2–3. 2003.

[26] S. M. Vanaki and H.A. Mohammed, Numerical study of nanofluid forced convection flow in channels using different shaped transverse ribs. Int. Communications Heat and Mass Transfer, 67(2015)176 -188.

NOMENCLATURE

a	rib height, mm
C_1, C_2, C_μ	empirical constant for turbulence model
C_p	specific heat, J/Kg k
D_h	hydraulic diameter, mm
d_p	particles diameter, nm
h	heat transfer coefficients, (W/m^2.^{o}C)
H	height of channel, mm
L	total length of channel, mm
L_1,L_3	lengths of unheated sections, mm
L_2	length of heated section, mm
f	friction factor
f_1, f_2, f_μ	damping function
k	turbulent kinetic energy, m/s^2
K	thermal conductivity, W/m. ^{o}C
N_t	dimensionless average entropy generation
Nu	Nusselt number
p	pressure, pa
PEC	thermal-hydraulic performance factor
q_w	heat flux, kW/m^2

Pr_t	Turbulent Prandtl number
Re	Reynolds number
S_g	Local entropy generation, $W/m^3.K$
T	temperature, ^oC
u ,v	velocities components, m/s
x, y	2D Cartesian coordinates, mm
P	rib to rib space,mm
b	width of rib ,mm

0	outlet
w	wall
x	local value

Greek Symbols

$\sigma_k, \sigma_\varepsilon$	empirical constant for turbulence model
ε	dissipation rate of turbulent kinetic energy
μ	dynamic viscosity, Ns/m^2
μ_t	turbulent dynamic viscosity, $N\ s/m^2$
ρ	density, kg/m^3
Δp	pressure drop, pa
Γ	Diffusion coefficient

Subscripts

av	average value
b	bulk fluid
eff	effective
f	base fluid
in	inlet
nf	nanofluid
p	particles
s	smooth channel